THE JOURNAL OF PHYSICAL CHEMISTRY B

Article

pubs.acs.org/JPCB

Influence of Solvent on Ion Aggregation and Transport in $PY_{15}TFSI$ Ionic Liquid–Aprotic Solvent Mixtures

Oleg Borodin,*[,†] Wesley A. Henderson,*[,‡] Eric T. Fox,[‡] Marc Berman,[§] Mallory Gobet,[§] and Steve Greenbaum[§]

[†]Electrochemistry Branch, Sensor & Electron Devices Directorate, U.S. Army Research Laboratory, Adelphi, Maryland 20783, United States

[‡]Ionic Liquids & Electrolytes for Energy Technologies (ILEET) Laboratory, Department of Chemical & Biomolecular Engineering, North Carolina State University, Raleigh, North Carolina 27695, United States

[§]Department of Physics & Astronomy, Hunter College of the City University of New York, New York, New York 10065, United States

Supporting Information

ABSTRACT: Molecular dynamics (MD) simulations using a many-body polarizable APPLE&P force field have been performed on mixtures of the *N*-methyl-*N*-pentylpyrrolidinium bis(trifluoromethanesulfonyl)imide ($PY_{15}TFSI$) ionic liquid (IL) with three molecular solvents: propylene carbonate (PC), dimethyl carbonate (DMC), and acetonitrile (AN). The MD simulations predict density, viscosity, and ionic conductivity values that agree well with the experimental results. In the solvent-rich regime, the ionic conductivity of the $PY_{15}TFSI$–AN mixtures was found to be significantly higher than the conductivity of the corresponding –PC and –DMC mixtures, despite the similar viscosity values obtained from both the MD simulations and experiments for the –DMC and –AN mixtures. The significantly lower conductivity of the $PY_{15}TFSI$–DMC mixtures, as compared to those for $PY_{15}TFSI$–AN, in the solvent-rich regime was attributed to the more extensive ion aggregation observed for the –DMC mixtures. The $PY_{15}TFSI$–DMC mixtures present an interesting case where the addition of the organic solvent to the IL results in an increase in the cation–anion correlations, in contrast to what is found for the mixtures with PC and AN, where ion motion became increasingly uncorrelated with addition of solvent. A combination of pfg-NMR and conductivity measurements confirmed the MD simulation predictions. Further insight into the molecular interactions and properties was also obtained using the MD simulations by examining the solvent distribution in the IL–solvent mixtures and the mixture excess properties.

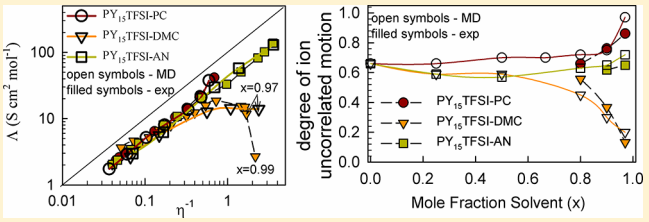

INTRODUCTION

Ionic liquids (ILs) have attracted significant attention over the last two decades, as many of them have a negligible vapor pressure, exceptional thermal and electrochemical stability, favorable dissolution properties with many organic/inorganic compounds, and low flammability.[1,2] ILs, which may consist of a diverse variety of cations and anions, have been widely investigated for a variety of applications including biphasic systems for separation, solvents for synthetic and catalytic applications,[3] lubricants,[4,5] lithium batteries,[6−8] supercapacitors,[9−11] actuators,[12,13] reaction media[14] replacement of conventional solvents,[2] and active pharmaceutical ingredients.[14] Importantly, IL properties can be tailored for specific chemical or electrochemical applications by tuning the combination of cations and anions to achieve the desired thermodynamic, solvating, and transport properties, as well as safety. Their relatively low ionic conductivity and high cost, however, present significant challenges to IL adoption for many electrochemical applications. The introduction of low viscosity solvents has therefore been explored in an effort to both improve the ion transport properties and reduce cost.

The availability of a large number of IL cations and anions, as well as organic solvents, presents tremendous opportunities for finding optimal cation/anion pairs and IL–solvent mixtures for the design of mixtures targeted toward specific applications. However, the screening of a large number of cation/anion and solvent combinations also presents an enormous challenge for product design, as the synthesis and characterization of a large number of ILs is expensive. Efficient and reliable predictive tools can speed up the development cycle not only by providing expedient predictions of properties for specific ILs and IL–solvent mixtures, but also by providing an improved fundamental understanding of the IL interactions and the data needed for the development of semiempirical structure–property relationship models. Molecular dynamics (MD)

Received: July 2, 2013
Revised: August 12, 2013
Published: August 13, 2013

   dx.doi.org/10.1021/jp406541e | J. Phys. Chem. B 2013, 117, 10581–10588

simulations are emerging as a powerful complementary option (to empirical correlations) for the reliable prediction of various properties of ILs. MD simulations also have the potential to provide insight needed for achieving a fundamental understanding of IL−solvent mixtures, as most structural, thermodynamic, and transport properties of ILs are readily accessible from simulations.[15−26]

This manuscript is a follow up to work recently reported consisting of a detailed experimental study of binary *N*-methyl-*N*-pentylpyrrolidinium bis(trifluoromethanesulfonyl)imide ($PY_{15}TFSI$) mixtures with numerous aprotic solvents that revealed a discrepancy between the conductivity and viscosity behavior in the solvent-rich regime.[27] Specifically, despite the similar viscosity of the $PY_{15}TFSI$ mixtures with acetonitrile (AN) and dimethyl carbonate (DMC), the conductivity of the $PY_{15}TFSI$−AN mixtures was significantly higher than the conductivity of the corresponding −DMC mixtures. On the other hand, similar conductivity values for the $PY_{15}TFSI$−DMC and −propylene carbonate (PC) mixtures were observed despite the large difference in the viscosity of the mixtures. Preliminary MD simulations suggested that quite different ion aggregation behavior of the $PY_{15}TFSI$ ions when mixed with PC, DMC, or AN is responsible for the discrepancies noted between the IL−solvent conductivity and viscosity.[27] Chaban et al. also recently reported an unusually high conductivity for 1-alkyl-3-methylimidazolium tetrafluoroborate ILs when mixed with AN, based upon MD simulations.[15] Couadou et al. also reported that trimethylsulfonium TFSI and trimethylammonium TFSI have a significantly higher conductivity when mixed with AN relative to similar mixtures with PC or γ-butyrolactone (GBL).[28]

In this manuscript, we have utilized MD simulations to obtain a fundamental understanding of the relationship between the viscosity, conductivity, structural, and thermodynamic properties of $PY_{15}TFSI$ mixed with the PC, DMC, and AN solvents shown in Figure 1. PC has a significantly higher viscosity than DMC and AN, while DMC has a significantly lower dielectric constant and dipole moments than PC and AN, as shown in Table 1. These solvents allow us to investigate the influence of both solvent polarity and viscosity on the properties of the IL−solvent mixtures.

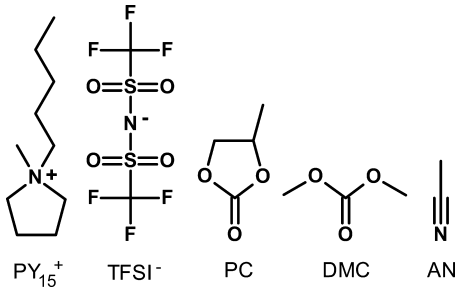

Figure 1. Structure of solvents and ions.

In this manuscript, the MD simulation predictions were validated against density, viscosity, and conductivity data. As ion association and correlated ion motion are central to the understanding of the IL−solvent conductivity behavior, it is especially important to ensure an accurate description of these factors for the IL−solvent mixtures. In order to further validate the MD simulation predictions for the ionic dissociation, a set of pfg-NMR self-diffusion coefficient measurements was performed and combined with the ionic conductivity data to yield the degree of ion dynamic correlation that is often called ionicity in the literature.[29]

Table 1. Solvent Properties: Viscosity (η) at 25 °C,[27] Dielectric Constant (ε)[27] at 25 °C, and Gas-Phase 0 K Dipole Moment from MP2/aug-cc-pvTz Calculations for the Low Energy Conformers of DMC and PC

solvent	η (mPa s)	ε	dipole (D)
PC	2.51	65.0	5.58
DMC	0.59	3.1	0.33
AN	0.34	36.0	3.94

EXPERIMENTAL AND COMPUTATIONAL SECTION

NMR experiments were run on a Varian direct drive 300 MHz spectrometer with a DOTY Z-gradient diffusion probe. All experiments were performed at 60 °C. A double stimulated echo pulse sequence was used to suppress convection effects, in conjunction with a saturation recovery sequence to shorten the data acquisition time. The data were collected and then fit to the equation to solve for the self-diffusion coefficient D:

$$I = I_0 \exp\left[D\gamma^2\delta^2 g^2\left(T + \frac{4\delta}{3} + 2\delta_{sp} + 2\tau\right)\right] \quad (1)$$

Here I is the signal integral and I_0 is a constant. The gradient values (g) used ranged up to 55 G cm^{-1}. Ring down times (τ) were 2 ms for all experiments. δ gradient durations were 2 ms for ^{1}H and 4 ms for ^{19}F experiments. T diffusion times were 66 ms for ^{1}H and 100 ms for ^{19}F experiments. δ_{sp}, the duration of the 80 G cm^{-1} spoiler gradient, was set to 2 ms. Further details for the NMR experiments and NMR spectra are given in the Supporting Information. The obtained diffusion coefficients for the $(1 - x_{solv})$ $PY_{15}TFSI$ + (x_{solv}) solvent mixtures (with PC, DMC, or AN; x_{solv} is the solvent mole fraction) are given in Table 2.

Table 2. Diffusion Coefficients of Solvent (D_{solv}), PY_{15}^+ (D_+), and $TFSI^-$ (D_-) for $(1 - x_{solv})$ $PY_{15}TFSI$ + (x_{solv}) S Mixtures (where S = AN, PC, and DMC) from NMR Measurements at 60 °C

solvent	x_{solv}	D_{solv} (10^{-9} m^2 s^{-1})	D_+ (10^{-9} m^2 s^{-1})	D_- (10^{-9} m^2 s^{-1})
PC	97	0.88	0.56	0.59
	90	0.62	0.44	0.43
	80	0.43	0.32	0.29
DMC	97	2.97	1.19	0.85
	90	1.93	0.64	0.74
	80	1.06	0.46	0.38
AN	97	4.57	2.39	2.27
	90	3.09	1.15	1.28

The previously developed many-body **A**tomistic **P**olarizable **P**otential for **L**iquids **E**lectrolytes and **P**olymers (APPLE&P) force field was used for $PY_{15}TFSI$ and the PC, DMC, and AN solvents.[30−33] *Lucretius*, an MD simulation package that includes many-body polarization, was used for all the MD simulations. The following solvent mole fractions were simulated for all $PY_{15}TFSI$−solvent mixtures: x_{solv} = 0, 0.25, 0.50, 0.80, 0.90, 0.97, and 1. An additional x_{solv} = 0.67 concentration was simulated for $PY_{15}TFSI$−PC mixtures. The PY_{15}^+ cations and $TFSI^-$ anions were dispersed in the simulation box at 120 °C by applying an additional repulsive

dx.doi.org/10.1021/jp406541e | J. Phys. Chem. B 2013, 117, 10581−10588

interaction between them. After the mixtures were equilibrated for 2−4 ns in the NPT ensemble at 120 °C, the simulation temperature was set to 60 °C and NPT runs were performed for 3.5−20 ns. The production runs were performed in the NVT ensemble for 8.2−44 ns depending on the IL concentration. The linear dimension of the simulation cell ranged from 38.4 to 51.7 Å. The Supporting Information lists the composition of the simulation cells, production and equilibration run length for each composition.

The Ewald summation method was used for the electrostatic interactions between permanent charges with permanent charges and permanent charges with induced dipole moments with $k = 8^3$ vectors. The Thole screening parameter of 0.2, as described in the force field section, was used. The interaction between an induced dipole and a partial charge separated by three bonds was scaled by 0.8, providing an improved description of the electrostatic potential around the molecules. Multiple time step integration was employed with an inner time step of 0.5 fs (bonded interactions); a central time step of 1.5 fs for all nonbonded interactions within a truncation distance of 7.0 Å and an outer time step of 3.0 fs for all nonbonded interactions between 7.0 Å and the nonbonded truncation distance of 13−14 Å; as well as for the reciprocal part of Ewald. The induced dipole−induced dipole interactions were scaled from full interactions to zero using the fourth order polynomial in the interval [13.5 Å, 14 Å] for a 14 Å cutoff or over [12.5 Å, 13 Å] in the case of a 13 Å cutoff. A Nosé−Hoover thermostat and a barostat were used to control the temperature and pressure with the associated frequencies of 10^{-2} and 0.1×10^{-4} fs. The stress tensor was saved every 9 fs for calculating stress, the tensor autocorrelation function, and viscosity, while the atomic coordinates were saved every 2 ps for postanalysis.

RESULTS AND DISCUSSION

Density. The density of the $PY_{15}TFSI$−solvent mixtures with PC, DMC, and AN solvents predicted from the MD simulations was found to be in good agreement with the measured data[27] for all of the studied solvent concentrations, as shown in Figure 2.

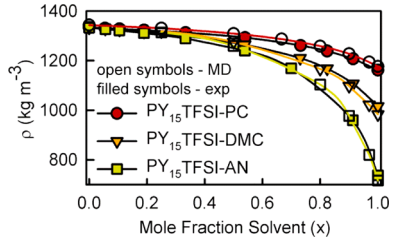

Figure 2. Density of $PY_{15}TFSI$−solvent binary mixtures from MD simulations and experiments.

Excess Volume. The nonideality of the mixtures can be measured through the excess thermodynamic properties. We probed the excess volume and energy of mixing of the mixtures using the MD simulations. The excess volume for the $PY_{15}TFSI$−solvent mixtures was negative for all of the compositions, as determined by both the MD simulations and experiments, as shown in Figure 3. The most negative values were observed for the $PY_{15}TFSI$−DMC mixtures, while the least negative (almost zero) values were observed for the $PY_{15}TFSI$−PC mixtures. It was previously found that large, relative to AN, cyclic molecules such as PC, EC, or GBL with a large dipole moment had the smallest excess volumes when mixed with $PY_{15}TFSI$, whereas less polar acyclic molecules tend to have the most negative excess volumes.[27] The magnitude of the observed excess volume for the $PY_{15}TFSI$−AN mixtures is similar to the previously reported values for $bmimBF_4$−AN mixtures.[34]

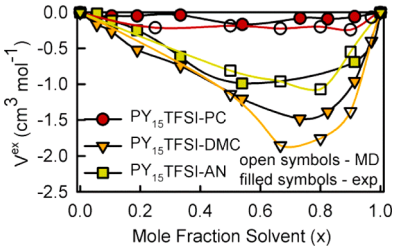

Figure 3. Excess volume (V^{ex}) for $PY_{15}TFSI$−solvent binary mixtures from MD simulations and experiments.

Excess Energy. The excess energy, calculated from MD simulations, is shown in Figure 4. The magnitude of the excess energy is small (<0.2 kJ mol^{-1}), indicating a similarity for the cation−anion and ion−solvent interactions. To put our predictions into perspective, we note that a positive excess enthalpy with a maximum of ∼1−2 kJ mol^{-1} was found for emimTriflate, $emimBF_4$, and $PY_{14}BF_4$ mixtures with water,[35] while mixtures of ILs having non-fluorinated ions, such as acetate or alkyl sulfate, with water resulted in more negative excess enthalpy values.[35−37] Previous experimental results for $bmimBF_4$ or $bmimMeSO_4$ mixtures with ethanol indicated maximum positive excess enthalpy values of ∼2.5 and 1.3 kJ mol^{-1}, respectively,[38] again following the trend that heavily fluorinated anions, such as BF_4^-, mixed with polar solvents tend to yield more positive heats of mixing. While $bmimBF_4$ and $bmimSO_4$ mixtures with ethanol had positive heats of mixing, the same mixtures with nitromethane resulted in the negative heats of mixing.[38]

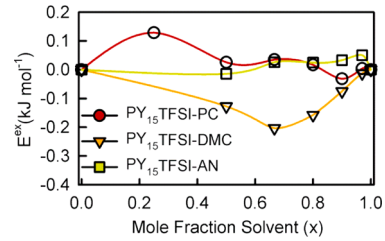

Figure 4. Excess energy (E^{ex}) for $PY_{15}TFSI$−solvent binary mixtures from MD simulations.

As the contribution of the ideal entropy of mixing to the free energy is always negative, the total entropic contribution is unlikely to be positive, yielding negative free energies of mixing values. Thus, our predicted very small energies of mixing are consistent with the experimentally observed mixing of IL solvents over the entire concentration range at 60 °C. Interestingly, there is a correlation between the excess volume and energy results shown in Figures 3 and 4—specifically, both properties are the most negative for $PY_{15}TFSI$−DMC and the most positive for $PY_{15}TFSI$−PC.

Viscosity. The viscosity of the $PY_{15}TFSI$−solvent mixtures was calculated using the Einstein relation, as discussed in the Supporting Information. The $PY_{15}TFSI$−solvent mixture viscosity values from the MD simulations and experiments[27]

dx.doi.org/10.1021/jp406541e | J. Phys. Chem. B 2013, 117, 10581−10588

are shown in Figure 5a. These data indicate that the viscosity of the $PY_{15}TFSI-PC$ mixtures is higher than that for the

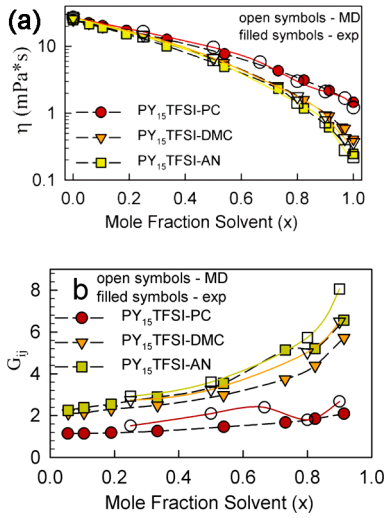

Figure 5. (a) Viscosity and (b) viscosity interaction parameter (G_{ij}) of $PY_{15}TFSI$–solvent mixtures from MD simulations and experiments.

$PY_{15}TFSI-DMC$ and $PY_{15}TFSI-AN$ mixtures, as would be expected from the order of increasing viscosity for the pure solvents. The excess viscosity is shown in the Supporting Information as Figure S7. It is negative for all of the mixtures and follows the order $PY_{15}TFSI-AN < PY_{15}TFSI-DMC < PY_{15}TFSI-PC$ both for the experimental results and MD simulations. A large negative excess viscosity was also previously reported for $bmimPF_6$–AN mixtures.[39]

One of the most widely used equations (eq 2) for predicting binary mixture viscosity is due to Grunberg and Nissan:[40]

$$\ln \eta_m = x_1 \ln \eta_1 + x_2 \ln \eta_2 + x_1 x_2 G_{ij} \quad (2)$$

where x_1 and x_2 are the molar fractions of components 1 and 2; η_1, η_2, and η_m are the viscosity of component 1, component 2, and the binary mixture, respectively; and G_{ij} is an interaction parameter that denotes the extent of nonideality of the system which is a function of the composition. G_{ij} was suggested to be related to the interchange energy arising from the increase in lattice activation energy due to juxtaposition of molecule 1 into the lattice of molecule 2.[41] If one replaces η_n in eq 2 with $\eta_n v_n$, where v_n is the molar volume of the nth component, then the term $x_1 x_2 G_{ij}$ is related to the molar Gibbs free energy of activation for the flow process in the Eyring absolute rate theory.[42] The G_{ij} parameter is plotted in Figure 5b. It is smallest for the $PY_{15}TFSI-PC$ mixtures and largest for the −AN mixtures. This ordering for the G_{ij} parameter weakly correlates with the order of excess volume shown in Figure 3. The increase of G_{ij} with increasing solvent mole fraction (x_{solv}) is attributed to the larger number of the ion–solvent contacts as the ion's first coordination shell gets filled upon addition of solvent up to x_{solv} = 0.90. This is consistent with the largest magnitude of excess volume being around x_{solv} = 0.80 (see Figure 3).

Ion Transport. Ion self-diffusion coefficients (D) and ionic conductivity (κ) was extracted using the Einstein relations shown in eqs 3 and 4:

$$D_i = \lim_{t\to\infty} \frac{1}{6} \sum_i^N \langle([\mathbf{R}_i(t) - \mathbf{R}_i(0)])^2 \quad (3)$$

$$\kappa = \lim_{t\to\infty} \frac{e^2}{6tVk_BT} \sum_{i,j}^N z_i z_j \langle([\mathbf{R}_i(t) - \mathbf{R}_i(0)])([\mathbf{R}_j(t) - \mathbf{R}_j(0)])\rangle \quad (4)$$

where e is the electron charge, V is the volume of the simulation box, k_B is Boltzmann's constant, T is the temperature, t is time, z_i and z_j are the charges over ions i and j in electrons, $R_i(t)$ is the displacement of ion i during time t, $\langle\ \rangle$ denotes the ensemble average, and N is the number of diffusing species in eq 3 and the sum of cations plus anions in the MD simulation cell in eq 4. Due to the finite size of the simulation cell, long-range hydrodynamic interactions restrict diffusion.[43] The leading order finite size correction (FSC) to the self-diffusion coefficient (change to delta ΔFSC) was found to be inversely proportional to the MD simulation box and is given by eq 5:[43]

$$\Delta D^{FSC} = \frac{2.837 k_B T}{6\pi\eta L} \quad (5)$$

where k_B is the Boltzmann constant, T is temperature, L is a linear dimension of the simulation periodic cell, and η is viscosity. The magnitude of FSC was 8–15% for solvents and 14–50% for ions with the largest values observed in dilute $PY_{15}TFSI-DMC$ solutions. The FSC was also applied to ionic conductivity by increasing it by the same amount as the ion diffusion coefficients were increased.

The ion diffusion coefficients predicted from the MD simulations are shown in Figure 6a, with excellent agreement

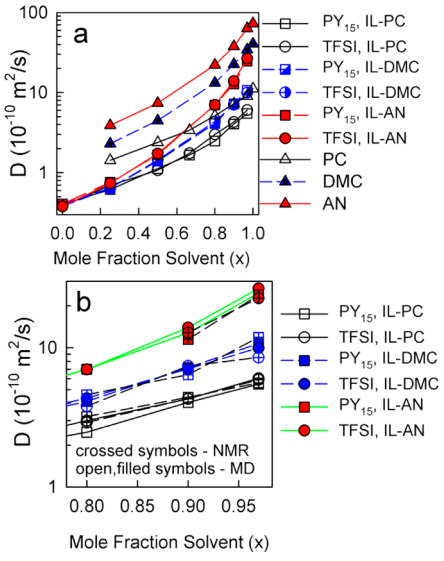

Figure 6. (a) Solvent and ion self-diffusion coefficients from MD simulations and (b) comparison of the ion self-diffusion coefficient from NMR and MD simulations.

between the MD simulation predictions and pfg-NMR measurements shown in Figure 6b. Solvent self-diffusion coefficients follow the inverse of the dependence of the viscosity, as expected, but the viscosity decreases faster upon solvent addition than the solvent diffusion coefficient increases, especially for the $PY_{15}TFSI-AN$ mixtures. The AN and DMC diffusion coefficients increase faster than the PC diffusion coefficient upon solvent addition, which is in line with the

dx.doi.org/10.1021/jp406541e | J. Phys. Chem. B 2013, 117, 10581–10588

viscosity behavior shown in Figure 5a. For the $PY_{15}TFSI$–DMC mixtures, the ion and solvent diffusion coefficients increase at the same rate, while the diffusion coefficients increase at a higher rate for the ions than for the solvents upon addition of solvent for the $PY_{15}TFSI$–AN and –PC mixtures, as shown in Figure S6 in the Supporting Information. At x_{solv} = 0.25, the ratios of the average ion diffusion coefficient to the solvent diffusion coefficient are 0.46, 0.29, and 0.19 for PC, DMC, and AN, respectively. This correlates with the sizes of the solvent molecules, which follow the order PC > DMC > AN. The order of the ratios of ion to solvent diffusion coefficients changes in the solvent-rich phase x_{solv} = 0.97, where the ratios are 0.64, 0.31, and 0.42 from the MD simulations and 0.65, 0.40, and 0.50 from the pfg-NMR experiments for PC, DMC, and AN, respectively. The fact that the addition of solvent increases the ion diffusion coefficients relative to the solvents for the –PC and –AN containing mixtures, but not for the $PY_{15}TFSI$–DMC mixtures is consistent with the PC and AN solvents effectively separating the ions, thus weakening the ion–ion interactions and increasing the ion diffusion coefficients, whereas DMC is less effective at the ion separation.

The ionic conductivity for the mixtures from the MD simulations and experiments is shown in Figure 7.[27] The MD

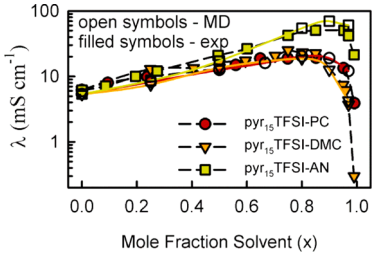

Figure 7. Ionic conductivity from MD simulations and from experiments.[27]

simulations not only accurately predict the correct position of the conductivity maximum, but also the magnitude of the conductivity for all of the concentrations. Notably, the conductivity of the $PY_{15}TFSI$–solvent mixtures does not follow the viscosity behavior shown in Figure 5. Specifically, from the mixture viscosity values, the conductivities of the $PY_{15}TFSI$–AN and –DMC mixtures are expected to be similar in magnitude with the conductivity of the –AN mixtures being only slightly higher than that for the –DMC mixtures. Instead, the conductivities of the $PY_{15}TFSI$–DMC and –PC mixtures are similar and significantly lower than the conductivity of the –AN mixtures.

In order to further examine the relationship between the conductivity and viscosity, the molar conductivity was plotted against fluidity (inverse of viscosity) in the Walden plot shown in Figure 8. The deviation from the ideal behavior line is commonly associated with the correlated ion motion and ion pair/aggregate formation. The $PY_{15}TFSI$–PC and –AN curves are parallel to the ideal line, indicating that the correlation of ion motion does not change upon addition of the solvent. The addition of DMC to $PY_{15}TFSI$, however, results in an increasing deviation from the ideal behavior as the solvent concentration increases past x_{solv} = 0.80.

The degree of ion uncorrelated motion (α_d) can be directly accessed from the MD simulations and a combination of pfg-NMR and conductivity measurements. It is also often called ionicity and is given by eqs 6 and 7:

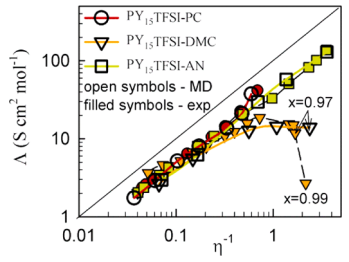

Figure 8. Walden plot showing inverse viscosity (η^{-1}) vs molar conductivity (Λ).

$$\alpha_d = \frac{\kappa}{\kappa_{uncorr}} \tag{6}$$

$$\kappa_{uncorr} = \frac{e^2}{VK_BT}(n_+D_+ + n_-D_-) \tag{7}$$

where e is the electron charge, V is the volume of the sample, k_B is Boltzmann's constant, T is the temperature, and n_+ and n_- are the number of cations or anions, respectively. κ_{uncorr} is the "ideal" conductivity that would be realized if ion motion were uncorrelated. The degree of ion uncorrelated motion from the MD simulations and experiments is shown in Figure 9. This

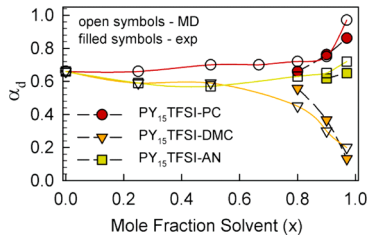

Figure 9. The degree of ion uncorrelated motion from MD simulations and experiments.

indicates that the MD simulations accurately capture the degree of ion correlations extracted from the combined experimental measurements. The degree of ion uncorrelated motion is essentially unchanged for the $PY_{15}TFSI$–AN mixtures over the entire concentration range studied. In the solvent-rich regime (x_{solv} > 0.80), the ionic motion in the $PY_{15}TFSI$–PC mixtures becomes slightly less correlated, while the correlation between the cation and anion diffusion dramatically increases for the $PY_{15}TFSI$–DMC mixtures, as reflected by the significant drop in α_d noted in Figure 9. A dramatic decrease of α_d was also observed by Tokuda et al.[44] for IL mixtures with a nonpolar solvent: *N*,*N*-diethyl-*N*-methoxyethyl-*N*-methyl ammonium $DEMEBF_4$ and DEMETFSI with 1,2-dichloroethane (DCE).

Structural Properties. Radial distribution functions (RDFs) of the $PY_{15}TFSI$–solvent mixtures were examined in order to better understand the relationship between the structural and transport properties. Figure 10 shows the center of mass cation–anion RDFs as a function of concentration. For the $PY_{15}TFSI$–PC and –AN mixtures, the first peak of the cation–anion RDFs is essentially unchanged from x_{solv} = 0.33 to 0.90, followed by a small increase for x_{solv} from 0.90 to 0.97. The behavior of the $PY_{15}TFSI$–DMC mixtures, however, is quantitatively different, with a significant increase in the first cation–anion peak noticeable for x_{solv} = 0.80. This is followed by a dramatic increase up to 15 upon a further increase of the DMC mole fraction up to x_{solv} = 0.97. The cation–anion RDF

dx.doi.org/10.1021/jp406541e | J. Phys. Chem. B 2013, 117, 10581–10588

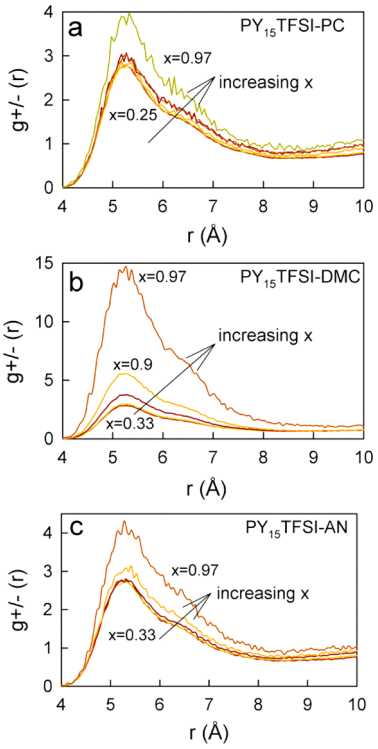

Figure 10. The cation−anion center of mass radial distribution functions from MD simulations.

behavior therefore correlates well with the increase in the correlation of the cation−anion motion observed for the $PY_{15}TFSI$−DMC mixtures, with little change in α_d for the other mixtures with −PC and −AN (see Figure 9).

Indeed, ion aggregation is quite pronounced in the simulation snapshot for the $PY_{15}TFSI$−DMC mixture shown in Figure 11b, with nanodomains of ion- and solvent-rich regions observed. In contrast, the ions are well dispersed in the $PY_{15}TFSI$−PC and −AN simulation cells shown in Figure 11a and c, which is consistent with the RDF behavior shown in Figure 10. We also examined the solvent aggregation in the IL-rich regime (x_{solv} = 0.33) and found that the magnitude of the first RDF peak is similar for the three solvents, having a value of 1.6−1.8. This indicates some moderate aggregation of solvent in the $PY_{15}TFSI$, as shown in more detail in the Supporting Information in Figure S10.

CONCLUSIONS

A detailed analysis of mixtures of the $PY_{15}TFSI$ IL with PC, DMC, and AN was performed using MD simulations, as well as viscosity, conductivity, density, and pfg-NMR experimental measurements. The $PY_{15}TFSI$−AN mixtures were found to have a much higher conductivity than the other two mixtures, despite the similar viscosity to the $PY_{15}TFSI$−DMC mixtures. The conductivity of the $PY_{15}TFSI$−PC mixtures was found to be similar to the $PY_{15}TFSI$−DMC mixtures, despite the much higher viscosity for the former. The viscosity and conductivity behavior was reconciled by the finding that significant ion aggregation occurs in the solvent-rich region for the $PY_{15}TFSI$−DMC mixtures, with the degree of ion uncorrelated motion (ionicity) dramatically decreasing from 0.6 to below 0.2 due to the formation of large transient aggregates as the mixture is further diluted with DMC. Thus, when the IL is mixed with low dielectric constant solvents, such as DMC, significant

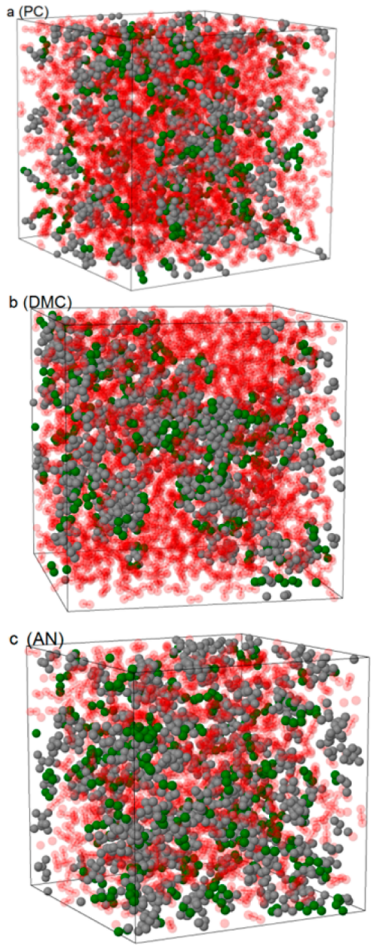

Figure 11. Snapshots of MD simulation box for x_{solv} = 0.90 for (1 − x_{solv}) $PY_{15}TFSI$−(x_{solv}) solvent with (a) PC, (b) DMC, and (c) AN. The solvent is transparent red, while the ions are opaque gray for the charged $TFSI^-$ anion and $N^+(CH_3)(CH_2)$ portion of the PY_{15}^+ cation and green for the neutral $-C_4H_9-$ and $-C_2H_4-$ portions of the PY_{15}^+ cation.

cation−anion aggregation is expected to occur in the solvent-rich regime. The most aggregated $PY_{15}TFSI$−DMC mixture counterintuitively had the most negative excess volume and excess energy amongst the three studied mixtures. These results indicate that the most negative excess volume and excess energy do not necessarily imply the strongest ion−solvent interactions and cannot be directly linked to ion dissociation because the excess properties are measured relative to the pure solvent and IL. For example, the most negative excess volume for the strongly aggregating $PY_{15}TFSI$−DMC mixture indicates that the ion aggregates fit DMC better than the solvated ions fit PC and AN.

The solvent diffusion coefficients increased to a lesser degree with increasing solvent concentration as compared to the increase of the mixture fluidity (inverse of viscosity) as the ion diffusion was slower than solvent diffusion. For the $PY_{15}TFSI$−PC and −AN mixtures, the ion diffusion increased at a higher rate than the solvent diffusion upon solvent addition due to an increase in the ion dissociation. In contrast, the ratio of the ion diffusion to solvent diffusion was essentially unchanged for the $PY_{15}TFSI$−DMC mixtures due to pronounced ion aggregation in the solvent-rich regime.

dx.doi.org/10.1021/jp406541e | J. Phys. Chem. B 2013, 117, 10581−10588

■ ASSOCIATED CONTENT

Supporting Information

Additional details for the NMR measurements; snapshots of the MD simulations for the $PY_{15}TFSI$ mixtures with PC, DMC, and AN; and details regarding the extraction of the viscosity data from the MD simulations. This material is available free of charge via the Internet at http://pubs.acs.org.

■ AUTHOR INFORMATION

Corresponding Authors

*E-mail: oleg.a.borodin.civ@mail.mil.
*E-mail: whender@ncsu.edu.

Notes

The authors declare no competing financial interest.

■ ACKNOWLEDGMENTS

The authors wish to express their gratitude to the U.S. Department of Energy (DOE) which fully supported the experimental part of this work. The modeling work at ARL was supported by the Multiscale Modeling Program. The NMR measurements were supported by the DOE Division of Materials Sciences & Engineering under award DE-SC0005029. The synthesis of the $PY_{15}TFSI$ and additional experimental measurements was supported by the DOE Division of Materials Chemistry under award DE-DC0001912.

■ REFERENCES

(1) Niedermeyer, H.; Hallett, J. P.; Villar-Garcia, I. J.; Hunt, P. A.; Welton, T. Mixtures of Ionic Liquids. *Chem. Soc. Rev.* **2012**, *41*, 7780−7802.

(2) Plechkova, N. V.; Seddon, K. R. Applications of Ionic Liquids in the Chemical Industry. *Chem. Soc. Rev.* **2008**, *37*, 123−150.

(3) Forsyth, S. A.; Pringle, J. M.; MacFarlane, D. R. Ionic Liquids - An Overview. *Aust. J. Chem.* **2004**, *57*, 113−119.

(4) Jin, C. M.; Ye, C. F.; Phillips, B. S.; Zabinski, J. S.; Liu, X. Q.; Liu, W. M.; Shreeve, J. M. Polyethylene Glycol Functionalized Dicationic Ionic Liquids with Alkyl or Polyfluoroalkyl Substituents as High Temperature Lubricants. *J. Mater. Chem.* **2006**, *16*, 1529−1535.

(5) Zeng, Z.; Phillips, B. S.; Xiao, J. C.; Shreeve, J. M. Polyfluoroalkyl, Polyethylene Glycol, 1,4-Bismethylenebenzene or 1,4-Bismethylene-2,3,5,6-Tetrafluorobenzene Bridged Functionalized Dicationic Ionic Liquids: Synthesis and Properties as High Temperature Lubricants. *Chem. Mater.* **2008**, *20*, 2719−2726.

(6) Shin, J. H.; Henderson, W. A.; Passerini, S. Ionic Liquids to the Rescue? Overcoming the Ionic Conductivity Limitations of Polymer Electrolytes. *Electrochem. Commun.* **2003**, *5*, 1016−1020.

(7) Garcia, B.; Lavallee, S.; Perron, G.; Michot, C.; Armand, M. Room Temperature Molten Salts as Lithium Battery Electrolyte. *Electrochim. Acta* **2004**, *49*, 4583−4588.

(8) Galinski, M.; Lewandowski, A.; Stepniak, I. Ionic Liquids as Electrolytes. *Electrochim. Acta* **2006**, *51*, 5567−5580.

(9) Vatamanu, J.; Borodin, O.; Smith, G. D. Molecular Insights into the Potential and Temperature Dependences of the Differential Capacitance of a Room-Temperature Ionic Liquid at Graphite Electrodes. *J. Am. Chem. Soc.* **2010**, *132*, 14825−14833.

(10) Kornyshev, A. A. Double-Layer in Ionic Liquids: Paradigm Change? *J. Phys. Chem. B* **2007**, *111*, 5545−5557.

(11) Zhu, Y.; Murali, S.; Stoller, M. D.; Ganesh, K. J.; Cai, W.; Ferreira, P. J.; Pirkle, A.; Wallace, R. M.; Cychosz, K. A.; Thommes, M.; Su, D.; Stach, E. A.; Ruoff, R. S. Carbon-Based Supercapacitors Produced by Activation of Graphene. *Science* **2011**, *332*, 1537−1541.

(12) Ding, J.; Zhou, D.; Spinks, G.; Wallace, G.; Forsyth, S.; Forsyth, M.; MacFarlane, D. Use of Ionic Liquids as Electrolytes in Electromechanical Actuator Systems Based on Inherently Conducting Polymers. *Chem. Mater.* **2003**, *15*, 2392−2398.

(13) Cho, M. S.; Seo, H. J.; Nam, J. D.; Choi, H. R.; Koo, J. C.; Song, K. G.; Lee, Y. A Solid State Actuator Based on the PEDOT/NBR System. *Sens. Actuators B* **2006**, *119*, 621−624.

(14) Hough, W. L.; Rogers, R. D. Ionic Liquids Then and Now: From Solvents to Materials to Active Pharmaceutical Ingredients. *Bull. Chem. Soc. Jpn.* **2007**, *80*, 2262−2269.

(15) Chaban, V. V.; Voroshyloya, I. V.; Kalugin, O. N.; Prezhdo, O. V. Acetonitrile Boosts Conductivity of Imidazolium Ionic Liquids. *J. Phys. Chem. B* **2012**, *116*, 7719−7727.

(16) Wu, X. P.; Liu, Z. P.; Huang, S. P.; Wang, W. C. Molecular Dynamics Simulation of Room-Temperature Ionic Liquid Mixture of [Bmim][BF_4] and Acetonitrile by a Refined Force Field. *Phys. Chem. Chem. Phys.* **2005**, *7*, 2771−2779.

(17) Liu, Z. P.; Wu, X. P.; Wang, W. C. A Novel United-Atom Force Field for Imidazolium-Based Ionic Liquids. *Phys. Chem. Chem. Phys.* **2006**, *8*, 1096−1104.

(18) Liu, H.; Sale, K. L.; Simmons, B. A.; Singh, S. Molecular Dynamics Study of Polysaccharides in Binary Solvent Mixtures of an Ionic Liquid and Water. *J. Phys. Chem. B* **2011**, *115*, 10251−10258.

(19) Scheers, J.; Pitawala, J.; Thebault, F.; Kim, J. K.; Ahn, J. H.; Matic, A.; Johansson, P.; Jacobsson, P. Ionic Liquids and Oligomer Electrolytes Based on the $B(CN)_4^-$ Anion; Ion Association, Physical and Electrochemical Properties. *Phys. Chem. Chem. Phys.* **2011**, *13*, 14953−14959.

(20) Schroder, C.; Neumayr, G.; Steinhauser, O. On the Collective Network of Ionic Liquid/Water Mixtures. III. Structural Analysis of Ionic Liquids on the Basis of Voronoi Decomposition. *J. Chem. Phys.* **2009**, *130*, 194503-1−194503-11.

(21) Spohr, H. V.; Patey, G. N. The Influence of Water on the Structural and Transport Properties of Model Ionic Liquids. *J. Chem. Phys.* **2010**, *132*, 234510-1−234510-12.

(22) Liu, H. J.; Maginn, E. An MD Study of the Applicability of the Walden Rule and the Nernst-Einstein Model for Ionic Liquids. *ChemPhysChem* **2012**, *13*, 1701−1707.

(23) Maginn, E. J. Molecular Simulation of Ionic Liquids: Current Status and Future Opportunities. *J. Phys.: Condens. Matter* **2009**, *21*, 373101-1−373101-17.

(24) Klähn, M.; Stüber, C.; Seduraman, A.; Wu, P. What Determines the Miscibility of Ionic Liquids with Water? Identification of the Underlying Factors to Enable a Straightforward Prediction. *J. Phys. Chem. B* **2010**, *114*, 2856−2868.

(25) Kashyap, H. K.; Annapureddy, H. V. R.; Raineri, F. O.; Margulis, C. J. How Is Charge Transport Different in Ionic Liquids and Electrolyte Solutions? *J. Phys. Chem. B* **2011**, *115*, 13212−13221.

(26) Kashyap, H. K.; Santos, C. S.; Daly, R. P.; Hettige, J. J.; Murthy, N. S.; Shirota, H.; Castner, E. W.; Margulis, C. J. How Does the Ionic Liquid Organizational Landscape Change When Nonpolar Cationic Alkyl Groups Are Replaced by Polar Isoelectronic Diethers? *J. Phys. Chem. B* **2013**, *117*, 1130−1135.

(27) Fox, E. T.; Paillard, E.; Borodin, O.; Henderson, W. A. Physicochemical Properties of Binary Ionic Liquid-Aprotic Solvent Electrolyte Mixtures. *J. Phys. Chem. C* **2013**, *117*, 78−84.

(28) Couadou, E.; Jacquemin, J.; Galiano, H.; Hardacre, C.; Anouti, M. A Comparative Study on the Thermophysical Properties for Two Bis[(trifluoromethyl)sulfonyl]imide-Based Ionic Liquids Containing the Trimethyl-Sulfonium or the Trimethyl-Ammonium Cation in Molecular Solvents. *J. Phys. Chem. B* **2013**, *117*, 1389−1402.

(29) Ueno, K.; Tokuda, H.; Watanabe, M. Ionicity in Ionic Liquids: Correlation with Ionic Structure and Physicochemical Properties. *Phys. Chem. Chem. Phys.* **2010**, *12*, 1649−1658.

(30) Borodin, O. Polarizable Force Field Development and Molecular Dynamics Simulations of Ionic Liquids. *J. Phys. Chem. B* **2009**, *113*, 11463−11478.

(31) Borodin, O.; Smith, G. D. Quantum Chemistry and Molecular Dynamics Simulation Study of Dimethyl Carbonate: Ethylene Carbonate Electrolytes Doped with $LiPF_6$. *J. Phys. Chem. B* **2009**, *113*, 1763−1776.

(32) Borodin, O.; Gorecki, W.; Smith, G. D.; Armand, M. Molecular Dynamics Simulation and Pulsed-Field Gradient NMR Studies of

Bis(fluorosulfonyl)imide (FSI) and Bis[(trifluoromethyl)sulfonyl]-imide (TFSI)-Based Ionic Liquids. *J. Phys. Chem. B* **2010**, *114*, 6786−6798.
(33) Borodin, O. Relation Between Heat of Vaporization, Ion Transport, Molar Volume, and Cation and Anion Binding Energy for Ionic Liquids. *J. Phys. Chem. B* **2009**, *113*, 12353−12357.
(34) Aliotta, F.; Ponterio, R. C.; Saija, F.; Salvato, G.; Triolo, A. Excess Thermodynamic Properties in Mixtures of a Representative Room-Temperature Ionic Liquid and Acetonitrile. *J. Phys. Chem. B* **2007**, *111*, 10202−10207.
(35) Ficke, L. E.; Brennecke, J. F. Interactions of Ionic Liquids and Water. *J. Phys. Chem. B* **2010**, *114*, 10496−10501.
(36) Ficke, L. E.; Novak, R. R.; Brennecke, J. F. Thermodynamic and Thermophysical Properties of Ionic Liquid + Water Systems. *J. Chem. Eng. Data* **2010**, *55*, 4946−4950.
(37) Katayanagi, H.; Nishikawa, K.; Shimozaki, H.; Miki, K.; Westh, P.; Koga, Y. Mixing Schemes in Ionic Liquid-H_2O Systems: A Thermodynamic Study. *J. Phys. Chem. B* **2004**, *108*, 19451−19457.
(38) Iglesias-Otero, M. A.; Troncoso, J.; Carballo, E.; Romaní, L. Densities and Excess Enthalpies for Ionic Liquids + Ethanol or + Nitromethane. *J. Chem. Eng. Data* **2008**, *53*, 1298−1301.
(39) Zafarani-Moattar, M. T.; Majdan-Cegincara, R. Viscosity, Density, Speed of Sound, and Refractive Index of Binary Mixtures of Organic Solvent Plus Ionic Liquid, 1-Butyl-3-methylimidazolium Hexafluorophosphate at 298.15 K. *J. Chem. Eng. Data* **2007**, *52*, 2359−2364.
(40) Poling, B. E.; Prausnitz, J. M.; O'Connell, J. P. *Properties of Gases and Liquids*, 5th ed.; McGraw-Hill: New York, 2001.
(41) Anantaraman, A. V. Thermodynamics of Solvent Mixtures. I. Density and Viscosity of Binary Mixtures of *N*-Methylpyrrolidinone − Tetrahydrofuran and Propylene Carbonate − Acetonitrile. *Can. J. Chem.* **1986**, *64*, 46−50.
(42) Martins, R. J.; Cardoso, M. J. E. D.; Barcia, O. E. Excess Gibbs Free Energy Model for Calculating the Viscosity of Binary Liquid Mixtures. *Ind. Eng. Chem. Res.* **2000**, *39*, 849−854.
(43) Dunweg, B.; Kremer, K. Molecular Dynamics Simulation of a Polymer Chain in Solution. *J. Chem. Phys.* **1993**, *99*, 6983−6997.
(44) Tokuda, H.; Baek, S. J.; Watanabe, M. Room-Temperature Ionic Liquid-Organic Solvent Mixtures: Conductivity and Ionic Association. *Electrochemistry* **2005**, *73*, 620−622.